Int J Adv Manuf Technol (2008) 36:606–617
DOI 10.1007/s00170-006-0863-1

ORIGINAL ARTICLE

Maximum allowable dynamic load of flexible mobile manipulators using finite element approach

M. H. Korayem · A. Heidari · A. Nikoobin

Received: 8 May 2006 / Accepted: 25 October 2006 / Published online: 10 January 2007

Abstract In this paper a general formula for finding the maximum allowable dynamic load (MADL) of flexible link mobile manipulators is presented. The main constraints used for the proposed algorithm are the actuator torque capacity and the limited error bound for the end-effector during motion on a given trajectory. The accuracy constraint is taken into account with two boundary lines which are equally offset due to the given end-effector trajectory, while a speed-torque characteristics curve of a typical DC motor, is used for applying the actuator torque constraint. Finite element method (FEM), which is able to consider the full nonlinear dynamic of mobile manipulator is applied to derive the kinematic and dynamic equations. In order to verify the effectiveness of the presented algorithm, two simulation studies considering a flexible two-link planar manipulator mounted on a mobile base are presented and the results are discussed.

Keywords Robot · Flexible link · Finite element · Maximum allowable dynamic load

1 Introduction

Flexible mobile robot manipulator systems exhibit many advantages over their traditional rigid arm counterparts: They require less material, have less arm weight, consume less power, are more maneuverable, require smaller actuators and are more transportable. Due to their extended workspace, mobile manipulators offer an efficient application for wide areas. But these systems are usually "power on board" with limited capacity. Hence, using light and small platforms and motor actuators in order to minimize the inertia and gravity effects on actuators will help a mobile manipulator to work in an energy-efficient manner. Using smaller actuators reduces the torque capacity of the actuators and limits the load carrying capacity of the robot.

Some studies exist on determining MADL for different types of robotic systems. Determination of maximum allowable dynamic load for manipulators has applications in advanced trajectory planning, design and selection of robot manipulators. For instance, Thomas et al. [1] used the load capacity as a criterion for sizing the actuator at the design stage of robotic manipulators and considered the maximum load in the neighborhood of a robot configuration. A technique was also developed in [2, 3] to maximize the MADL of an entire trajectory, rather than in the neighborhood of a configuration. In these works, piecewise rigid links and joints were assumed. Korayem and Basu [4, 5] presented an algorithm for computing the MADL of elastic manipulators by relaxing the rigid body assumption. The maximum payload of kinematically redundant manipulators is computed using a finite element method for describing the dynamics of a system by Yue et al. [6]. Korayem and Ghariblu developed an algorithm for finding the MADL of rigid mobile manipulators [7]. There is also some research on carrying heavy loads or the application of large forces by mobile manipulators [8, 9]. Different types of constraints have been applied to a robotic system in order to solve the redundancy resolution [10, 11]. None of these published works have considered finding the MADL on mobile manipulators using finite element approach including kinematic redundancy. The finite element method has been used to solve very

M. H. Korayem (✉) · A. Heidari · A. Nikoobin
Robotic Research Laboratory, Mechanical Engineering Department, Iran University of Science and Technology, Tehran, Iran
e-mail: hkorayem@iust.ac.ir

complex structural engineering problems during the past years. One of the main advantages of FEM over the most of other approximate solution methods is the fact that FEM can handle irregular geometries routinely. Another significant advantage of FEM, especially over analytical solution techniques is the ease with which nonlinear conditions can be handled.

The main focus of this paper is on mobile elastic link manipulators. A brief introduction to the dynamics of these types of systems is being reviewed. A strategy for determining the MADL subject to both constraints is described, where a series of ball-type bounds centered at the desired trajectory is used for defining the end-effector oscillation constraint, and motor speed-torque characteristics curve of a typical DC motor is used in actuator constraint. A computational procedure is then presented which allows the computation of the MADL for an arbitrary prescribed dynamic motion of the end-effector. Finally, two numerical examples involving a two link flexible mobile manipulator are presented and results are discussed.

2 Model development approach

The overall approach involves treating each link of the manipulator as an assemblage of ni elements of length l_i. For each of these elements the kinetic energy T_{ij} and potential energy V_{ij} are computed in terms of a selected system of n generalized variables $q=(q_1, q_2, ...q_n)$ and their rate of change $\dot{q}$. These energies are then combined to obtain the total kinetic energy, T, and potential energy, V, for the entire system. For the sake of massive calculation, above-mentioned procedure is presented in Appendix (A-1) to (A-3).

Dynamic equations for systems are derived through the Lagrange equations:

$$\frac{d}{dt}\left(\frac{\partial £}{\partial \dot{q}_k}\right) - \frac{\partial £}{\partial q_k} = Q_k,\ k = 1, 2, ...n \tag{1}$$

where $£ = T - V$.

Equation (1) along with associated boundary conditions (Appendix A-4) provides the desired dynamic equations of system as follows:

$$M\ddot{q} - f = Q \tag{2}$$

where M=M(q) and $f = f\left(q, \dot{q}\right)$ are nonlinear functions of generalized variables q, and their rate of change $\dot{q}$. Q denotes the applied torque at each joint.

3 Dynamic model of flexible robot manipulator

From Eqs. (A-28) and (A-30), the Lagrangian of link 1 is as follow:

$$£_1 = T_1 - V_1 = \frac{1}{2}\dot{q}_1^T M_1 \dot{q}_1 - m_1 g[0 \quad 1] T_0^1 \begin{bmatrix} \frac{1}{2} n_1^2 l_1^2 \\ R_0 \psi_1 \end{bmatrix} - \frac{1}{2}\psi_1^T K_1 \psi_1. \tag{3}$$

From Eqs. (A-29), (A-31), the Lagrangian of link 2 can be derived:

$$£_2 = \frac{1}{2}\dot{q}_2^T M_2 \dot{q}_2 - m_2 g[0 \quad 1] T_0^1 \left[\begin{bmatrix} L_1 \\ u_{2n_1+1} \end{bmatrix} n_2 l_2 + T_1^2 \begin{bmatrix} \frac{1}{2} n_2^2 l_2^2 \\ R_1 \psi_2 \end{bmatrix} \right] - \frac{1}{2}\psi_2^T K_2 \psi_2. \tag{4}$$

The overall Lagrangian for a two-link flexible mobile manipulator with the base motion in x direction can then be written as:

$$£ = £_1(x_0, \theta_1, u_3, u_4, ...u_{2n_1+2}) + £_2(x_0, \theta_1, u_{2n_1+1}, u_{2n_1+2}, \theta_2, w_3, w_4, ...w_{2n_2+2}). \tag{5}$$

By applying Lagrange's equation and performing some algebraic manipulations, the compact form of the system's dynamic equations becomes:

$$\sum_{j=1}^{n} M_{ij}\ddot{q}_j + \sum_{j=1}^{n}\sum_{k=1}^{n_j} h_{ijk}\dot{q}_j\dot{q}_k = R_i \quad (i = 1, 2, .., n) \tag{6}$$

$$\sum_{j=1}^{n} M_{f,ij}\ddot{q}_j + \sum_{j=1}^{n}\sum_{k=1}^{n} h_{f,ijk}\dot{q}_j\dot{q}_k = R_{f,j} \tag{7}$$

where M, the inertia matrix, is consisted of element coefficients related with the second derivative of generalized variables, $\ddot{q}$. h considers the contribution of other dynamic forces such as centrifugal and Coriolis forces while R consists of gravity and other external forces. Dynamic Eqs. (6) and (7) are arranged on joint variables and deflections. Equation (6) concerns the joints rotation in robot and Eq. (7) specifies the elastic deformation in links [7].

4 Modification of the model

The extension of the model to a case where a load m_l is added at the tip of the manipulator can be carried out. For

computing the kinetic and potential energies of the tip mass, the end-effector position $\overrightarrow{r}_m$ can be expressed as follows:

$$\overrightarrow{r}_m = \begin{Bmatrix} x_0 \\ 0 \end{Bmatrix} + T_0^1 \left[\begin{bmatrix} L_1 \\ u_{2n_1+1} \end{bmatrix} + T_1^2 \begin{bmatrix} L_2 \\ u_{2n_2+1} \end{bmatrix} \right]. \tag{8}$$

After computing these energies, they can be added to the total energy of robot in Lagrange equation. One can show that the matrix differential model of the overall system in the matrix form, with manipulator at the tip is of the form:

$$M_T \ddot{q} - f_T = Q_T \tag{9}$$

where

$$M_T = M + M_m, f_T = f + f_m, Q_T = Q + Q_m \tag{10}$$

and the subscript 'T' refers to the total system, and subscript 'm' represents the influence of the additional mass.

5 Kinematic model of flexible link mobile manipulator

Inverse kinematic can be used to derive the generalized variables (q) for a predefined trajectory which is useful in our following calculations for finding the MADL. If the vector of position of the end-effector is considered to be $\overrightarrow{P} = X\left(q_r, q_f\right)^T$, then taking derivative with respect to time will yield the velocity of the end-effector:

$$\dot{\overrightarrow{P}} = \left[J_r, J_f\right]\left(\dot{\overrightarrow{q}}_r, \dot{\overrightarrow{q}}_f\right)^T = J\dot{\overrightarrow{q}} \tag{11}$$

where q_r, q_f are generalized variables and J_f, J_r are the Jacobian matrices of the mobile robot manipulator of joints rotation and deflection in links, respectively. After taking the derivative of Eq. (11) with respect to time, we can express equations of the end-effector's acceleration as:

$$\begin{aligned} \ddot{\overrightarrow{P}} &= \left[J_r, J_f\right]\left(\ddot{\overrightarrow{q}}_r, \ddot{\overrightarrow{q}}_f\right)^T + \left[\dot{J}_r, \dot{J}_f\right]\left(\dot{\overrightarrow{q}}_r, \dot{\overrightarrow{q}}_f\right)^T \\ &= J\ddot{\overrightarrow{q}} + \dot{J}\dot{\overrightarrow{q}} \end{aligned} \tag{12}$$

When the end-effector trajectory $\left(\overrightarrow{p}, \dot{\overrightarrow{p}}, \ddot{\overrightarrow{p}}\right)$ is predefined, the generalized coordinates of motion and their derivations $\left(\overrightarrow{q}, \dot{\overrightarrow{q}}, \ddot{\overrightarrow{q}}\right)$, can be derived with inverting Eq. (12). $J \in R^{3\times s}$ is not square and cannot be inverted directly. In other words, the number of equations is less than the number of unknowns in Eq. (12) and as a result, for inverting this equation and finding J^{-1}, some additional equations are required as a complementary set. The first choice is dynamic equations related to the deflection of the links. Adding these equations to Eq. (12) and rearranging the obtained equations will result the following form:

$$\begin{aligned} &\left(\ddot{\overrightarrow{q}}_r, \ddot{\overrightarrow{q}}_f\right)^T \\ &= \left[J_r, J_f\right]^{-1}\left(\ddot{\overrightarrow{P}} - \left[\dot{J}_r, \dot{J}_f\right]\left(\dot{\overrightarrow{q}}_r, \dot{\overrightarrow{q}}_f\right)^T\right) \\ &= J^{-1}\left(\ddot{\overrightarrow{P}} - \dot{J}\dot{\overrightarrow{q}}^T\right) \end{aligned} \tag{13}$$

In this case, the number of equations is less than the number of unknowns in Eq. (12); therefore, for inverting this equation and finding J^{-1} in Eq. (13) some additional equations are required as a complementary set. The first choice is dynamic equations that are governed on nodes of elements in FEM in the elastic link Eq. (7).

The resulting equations Eq. (13) are not only highly coupled and nonlinear, but also too lengthy, which makes it extremely difficult to handle manually even for a less degree of freedom manipulator with a low number of elements.

6 Formulation of MADL for a predefined trajectory

The MADL of a flexible link mobile manipulator is defined as the maximum load which the mobile manipulator can carry in performing the trajectory with acceptable precision for a pre-defined trajectory [7]. The emphasis on the tracking accuracy is due to relaxation of the rigid body assumption and to the fact that one of the main reasons for the deviation from the desired trajectory is the flexibility in links. This can be taken into account in MADL determination by imposing a constraint on the end-effector deflection, in addition to the actuator torque constraint. Deflection of the end-effector can cause excessive deflection from the pre-defined trajectory, even though the joint torque constraint is not violated. By considering the actuator torque and deflection constraints and adopting a logical computing method, the maximum load carrying capacity of a mobile manipulator for a given trajectory can be computed. The algorithm is proposed for finding the MADL of the system as shown in Fig. 1.

This algorithm illustrates computing procedure for finding MADL by considering the manipulator workspace and end-effector trajectory. The dynamic equations by considering of an initial load are solved. Then, the actuator torque and accuracy coefficients are computed for each point of the discretised trajectory to find the associated MADL. The computed MADL of each point can be plotted versus the corresponding time. The minimum value of this curve specifies the maximum dynamic load of robot manipulator. If the difference between specified values for

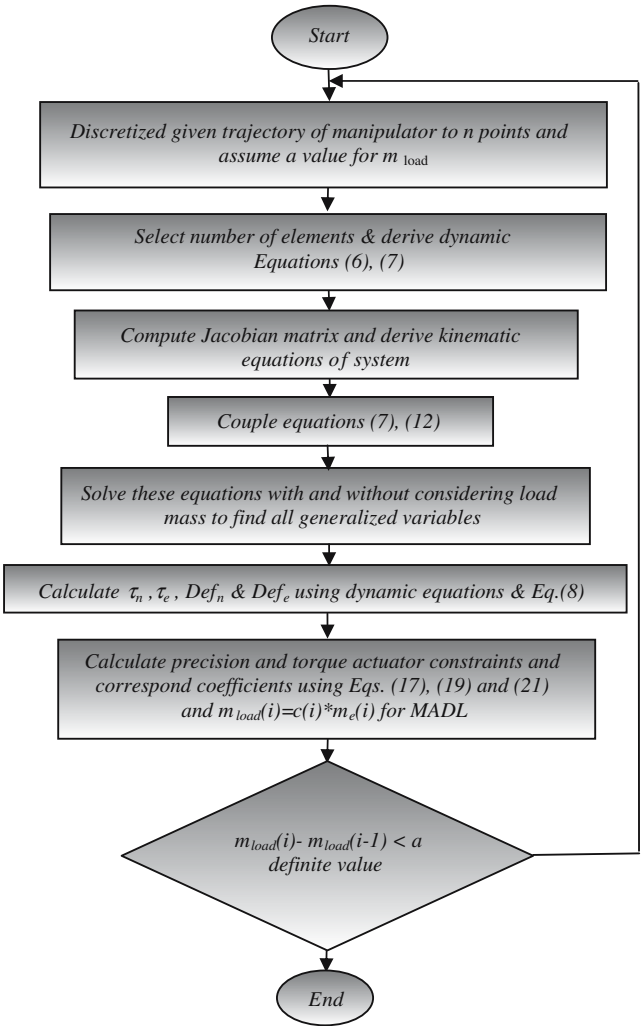

Fig. 1 Flowchart of the computational procedure

ml in two loops is less than a definite value, which is specified by the user, the specified MADL will be exact, otherwise the program jumps back to the first step and a new initial mass of load ml is selected until all constraints are satisfied.

7 Formulation of actuator torque constraint

The joint actuator torque constraint was formulated based on the typical torque-speed characteristics of DC motors [7]. Other actuation systems can be dealt with similarly.

$$U^{+} = k_1 - k_2\dot{q}$$
$$U^{-} = -k_1 - k_2\dot{q} \tag{14}$$

where, $k_1=T_s$, $k_2=T_s/\omega_{nl}$, T_s is the stall torque and ω_{nl} is the maximum no load speed of the motor. U^{+} and U^{-} are the upper and lower bounds of the allowable torque. Using the computational procedure the ith joint torque due to the dynamics of a mobile vehicle and an n-link manipulator and load can be computed for each point of the discretised trajectory $(\tau_e)_i$, i=1, 2,... , n+m. Also, using Eq. (14) the upper and lower bounds of motor torques can be found and the available torque for the carrying load is then

$$\tau_i^{+} = (U^{+})_i - (\tau_l)_i,$$
$$\tau_i^{-} = (U^{-})_i - (\tau_l)_i. \tag{15}$$

The maximum allowable torque at the ith joint is equal to:

$$\tau_i^{+} = \max\left\{\tau_i^{+}, \tau_i^{-}\right\} \tag{16}$$

Equation (16) remains valid for flexible manipulators because the linearity between the force F acting on the end-effector (a load can be modeled as an inertial force on the tip) and corresponding joint torques τ is preserved if small deformations are assumed. Therefore, it is necessary to introduce the concept of a load coefficient complying with the actuator torque constraint which can be calculated for each point j, of a given trajectory as follows:

$$(C_a)_j = \frac{\left|(\tau_{\max})_j - (\tau_{nl})_j\right|}{(\tau_l)_j} \qquad j = 1, 2, ..., m \tag{17}$$

where τ_{nl} is the no-load torque. Physically, the load coefficient $(C_a)_j$ on the *j*th joint actuator describes the accessible torque for carrying the maximum load to the torque which is applied for carrying the initial load.

8 Formulation of accuracy constraint

Deflection at end-effector could be attributed to both static and dynamic factors, such as, link flexibility, joint clearance, manipulator and load inertia. These factors are configuration dependent and for this, MADL varies from place to place on a given dynamic trajectory. A constraint should be imposed in such a way that the worst case, which corresponds to the least MADL, is used to determine the maximum allowable load.

A given trajectory is first digitized into manipulator points. No load deflection $(Def_n)_j$ and deflection with added end-effector mass $(Def_e)_j$ are calculated for j=1,2,...,m,

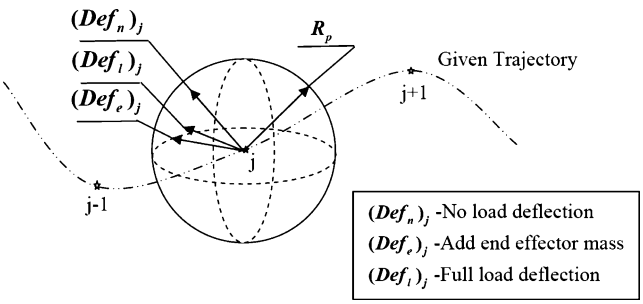

Fig. 2 Spherical boundary of end-effector deflection [7]

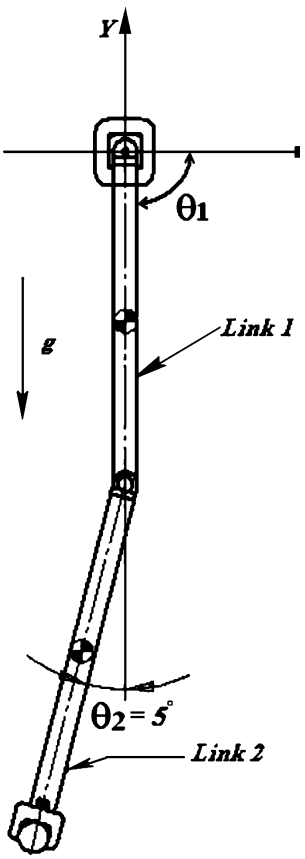

Fig. 3 Initial condition for the simulation

using the computational procedure outlined in Appendix and Eq. (8). As seen in Fig. 2, the additional mass at the end-effector changes both the magnitude and the direction of the deflection. But as long as the magnitude of the deflection is less or equal to an allowable value, the robot is considered to remain capable of executing the given trajectory. In other words, only the magnitude of deflection $(Def_n)_j$ and $(Def_e)_j$ need to be considered.

This prompted the use of a spherical boundary of radius R_p as the end-effector deflection constraint and the sphere is centered at the desired position on the given trajectory. Although $(Def_{nl})_j$ and $(Def_e)_j$ are generally vectors of different directions, the magnitude increase due to the added mass at the end-effector is linearly related to the mass [7]. Therefore, the difference between the allowable

Table 1 Simulation of parameters

Parameter	Value	Unit
Length of links	$L_1=L_2=1.414$	m
Mass	$m_1=0.7$, $m_2=0.5$	Kg
Moment of inertia	$I_1=I_2=5.5e\text{-}4$	$Kg.m^2$
Spring constant	$K_1=15$, $K_2=10$	N.m
Actuator stall torque	$Ks_1=18, Ks_2=25$	Nm.s/rad

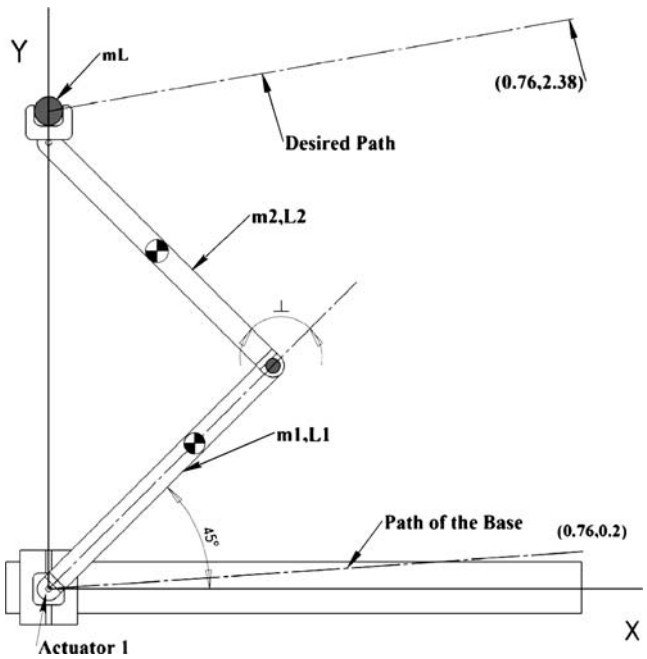

Fig. 4 Schematic of robot and the desired path of end-effector

deflection and the magnitude of deflection by added end-effector mass at point j:

$$R_p - (Def_e)_j \tag{18}$$

can be regarded as the remaining amount of end-effector deflection which can still be accommodated at point j of the given trajectory. This remaining amount indicates how much load can be carried through the point j without violating the deflection constraint. Therefore it is necessary to introduce the concept of a load coefficient $(C_a)_j$ for point j, j=1,2,...m, as follows:

$$(C_a)_j = \frac{R_p - (Def_e)_j}{\max\{Def_e\} - \max\{Def_n\}} \tag{19}$$

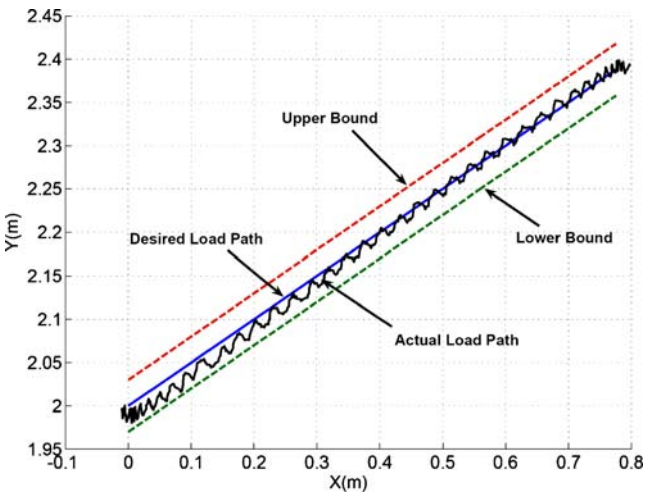

Fig. 5 The desired and the actual load path

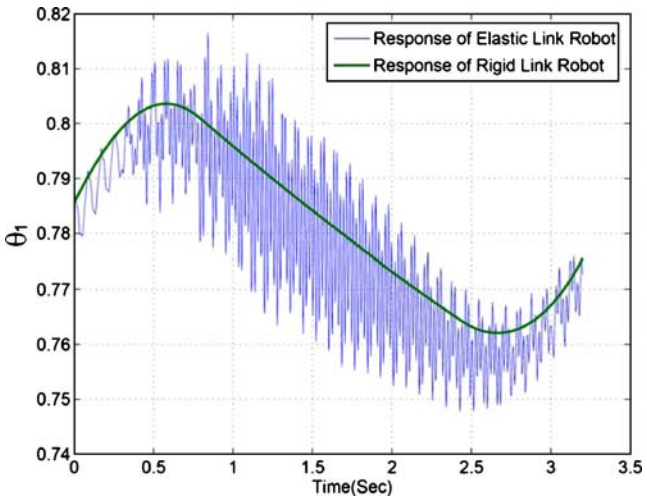

Fig. 6 Joint responses of θ_1 for rigid and flexible links

where

$$\max\{Def_e\} = \max\left\{(Def_e)_1, (Def_e)_2, ..., (Def_e)_m\right\}$$
$$\max\{Def_n\} = \max\left\{(Def_n)_1, (Def_n)_2, ..., (Def_n)_m\right\}. \quad (20)$$

Finally the load coefficient (c) can be obtained as follows:

$$c = \min\left\{(c_p)_j, (c_a)_j\right\}, j = 1, 2, ..., m. \quad (21)$$

Then, the maximum mass that can be carried on the given trajectory is $m_{load} = c \times m_e$.

9 Simulation results and discussion

In order to initially check the validity of the presented model, the response of the system, with a high elastic constant (EI), at the initial conditions corresponding to θ_1=−90 deg and θ_2= 5 deg (Fig. 3) is simulated. The response of the system is in agreement with the harmonic motion of an inelastic two-link robot hanging freely under gravity. This problem is performed again after considering the elasticity in links. The results are in good agreement with a similar case done in [12].

Two additional simulations of the system are performed. In the first test, a robot manipulator with elastic links is considered. The end-effector and its load must track a straight line with a predefined speed. In the second test, MADL is found for a flexible robot manipulator in which end-effector must move along a circular path. In both cases, the mobile base of manipulator moves along a straight line with a constant speed.

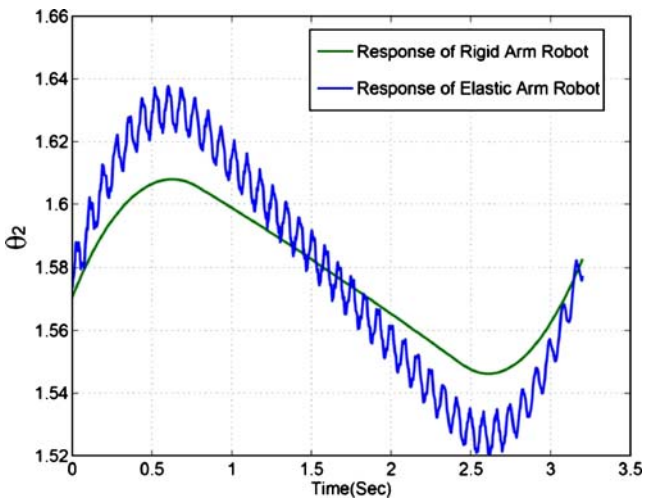

Fig. 7 Joint responses of θ_2 for rigid and flexible links

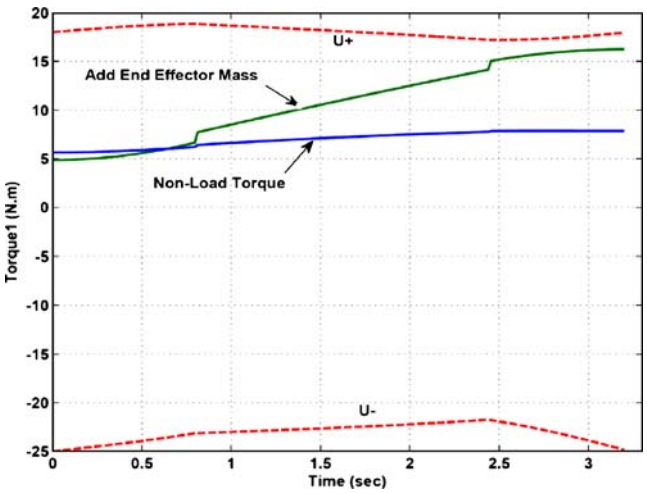

Fig. 8 Applied torques of the first motor

9.1 Test 1: MADL of a flexible mobile robot manipulator with a linear path

This simulation study is performed to investigate the efficiency of the procedure presented in Fig. 1 for

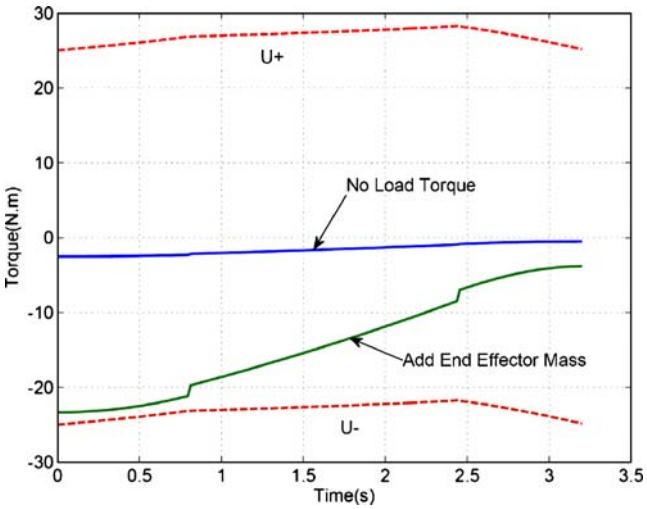

Fig. 9 Applied torques of the second motor

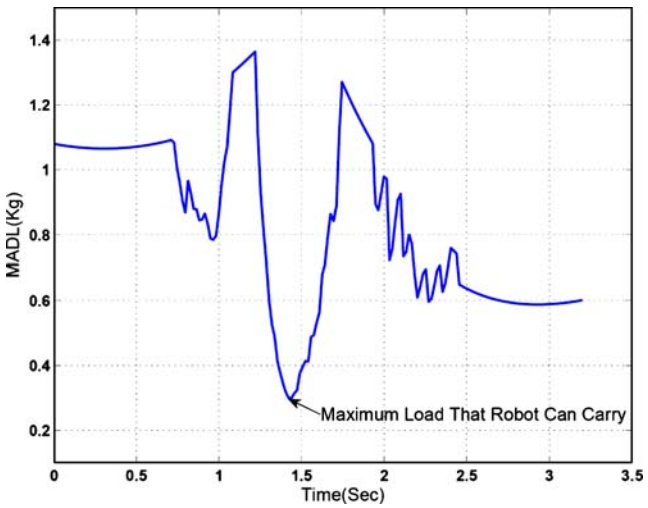

Fig. 10 Maximum allowable dynamic load (MADL)

computing the maximum allowable load of a mobile manipulator. All required parameters are given in Table 1.

As mentioned earlier, the path of end-effector and its payload is linear which starts from point (x_1=0, y_1=2 m) and ends at a point with coordinate (x_2=0.76 m, y_2=2.38 m) (Fig. 4). The velocity profile of the end-effector is as below:

$$\begin{cases} v = at & 0 \le t \le T/4 \\ v = v_{\max} & T/4 \le t \le 3T/4 \\ v = -at & 3T/4 \le t \le T \end{cases} \quad (22)$$

The permissible error bound for the load motion around the desired path is limited to Re=0.03 m. A linear path is planed for the vehicle, which starts from the origin and ends at (x_{b2}= 0.76 m, y_{b2}=0.2 m) with the velocity of V_b=0.5 t. The obtained path of the end-effector, considering link flexibility is shown in Fig. 5 in comparison with the desired path. Also the joint angles of rigid and flexible link states are shown in Figs. 6 and 7. The corresponding applied torques to the manipulator actuators, are shown in Figs. 8 and 9. Finally, Fig. 10 depicts the maximum load which can be carried by the robot versus the total time for the final motion. Minimum of this graph shows the maximum allowable dynamic load of the robot system which is 0.25 kg.

9.2 Test 2: MADL of a flexible mobile robot manipulator with a circular path

In this simulation, the computation of the MADL for a two-link planar manipulator mounted on an XY table (Fig. 11) is presented. The link parameters and inertia properties of the manipulator were given in Table 2. In the inertial reference frame, the XY table is capable of moving 1000 mm along the X-axis and 200 mm along the Y-axis. Base velocity is V_x=0.5 t. Also, it is assumed that the load must move along a circular path. The centre of the circular path coordinates with a radius r=50 cm, is at (x_c=1 m; y_c= 1 m) with origin at the lower-left corner of the XY table (Fig. 12). The angular velocity of the end-effector is 180 deg /s with an overall time of the motion 1.5 s. By this initial condition (given time and angular velocity) only 3/4 of a full circle will be tracked.

The base work space (BWS) was discretised into 20 equally-distance points in both traversing directions and into 40 points in the load trajectory. The maximum allowable error-bound at each point of the desired path must lie on a sphere with the radius of 5 cm.

The obtained path which is tracked by the flexible robot manipulator is compared with the desired path in Fig. 12. The graph shows that, the accuracy constraint is violated

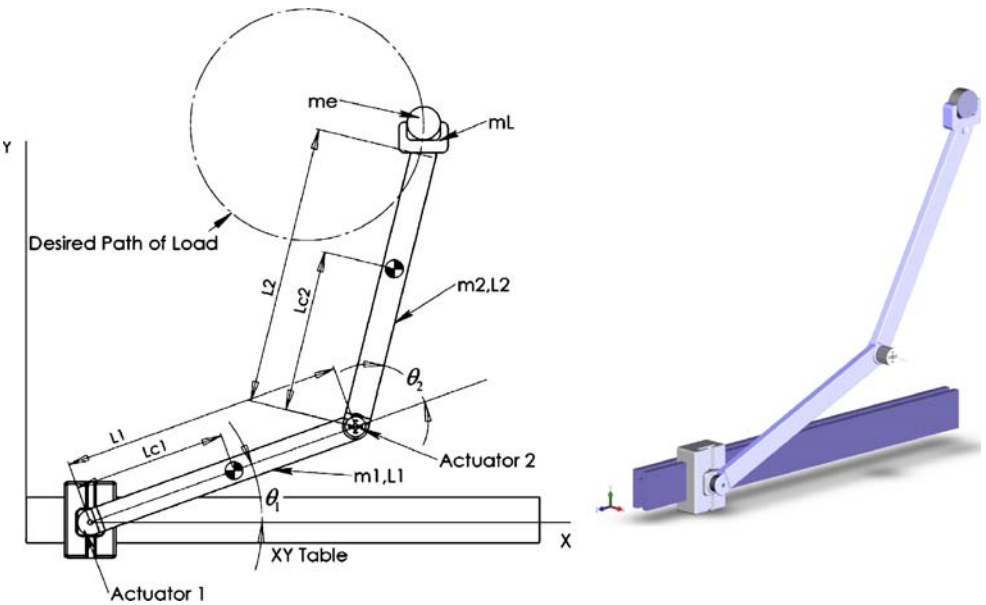

Fig. 11 Schematic view of the flexible link planar manipulator with mobile base

Table 2 Parameters of two-link planar flexible manipulator

Parameter	Value	Unit
Length of links	$L_1=L_2=1.2$	m
Mass	$m_1=0.80$, $m_2=0.80$	Kg
Moment of inertia	$I_1=I_2=5.5e\text{-}4$	$Kg.m^2$
Spring constant	$K_1=17$, $K_2=12$	N.m
Actuator stall torque	$Ks_1=12$,$Ks_2=30$	Nm.s/rad

between t=0.8 s and t=1.38 s. It can be concluded that the assumed value for m_{load} is more than the robot allowable dynamic load and so another value for m_{load} must be chosen. After correcting this value, the obtained load trajectory satisfies the precision constraint.

Joint angles of rigid and flexible link robots are shown in Figs. 13 and 14, for the final motion. The equivalent maximum dynamic load versus time is shown in Fig. 15. In this case, the maximum dynamic load is found to be 0.54 kg.

10 Conclusions

The main objective of this study was formulating the MADL and determining the maximum allowable dynamic load for flexible-link manipulators with a pre-defined trajectory, using the finite element method. This was achieved by imposing actuator torque capacity and end-effector accuracy constraints to the problem formulation. In simulation studies a two-arm planar manipulator mounted on a mobile base was considered for carrying a load on two predefined trajectory and examined in two test cases.

In the first case, none of the joint motors are required to move at its full capacity until just before t=2.5 s when torque in the joint 1 increases and approaches the upper bound. It can be concluded that actuator torque capacity is the dominant constraint for determining the maximum allowable load of the motion because the elastic trajectory is almost far from the bounds, and then the precision constraint is not the determining factor in this case. In the second case, the maximum dynamic load is determined to be 0.54 kg in t=0.9 s. In the first attempt, the accuracy of the end-effector is violated. As mentioned in the procedure of finding the MADL, either m_{load} can be modified on the second try or the base trajectory can be changed without changing the end-effector trajectory. Therefore, in the mobile base manipulator there is another alternative for carrying more loads in comparison with fixed base robots.

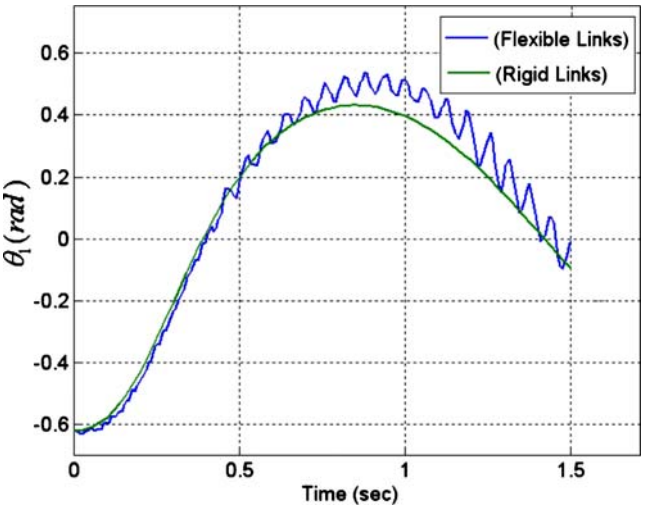

Fig. 13 Joint responses of θ_1 for rigid and flexible links

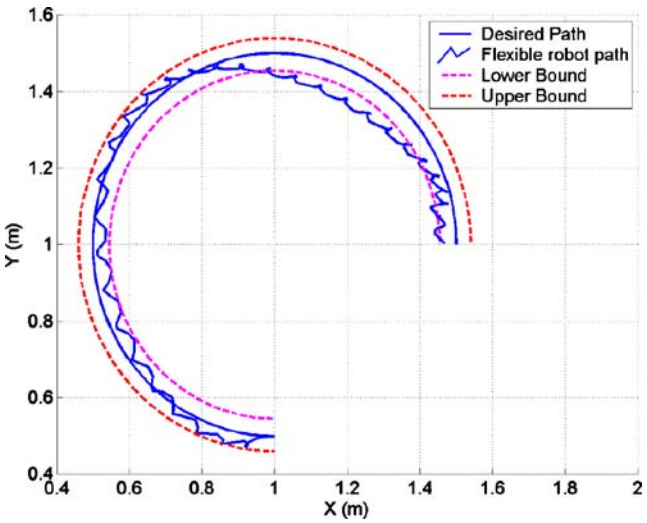

Fig. 12 Comparison of flexible joint robot path with respect to desired path

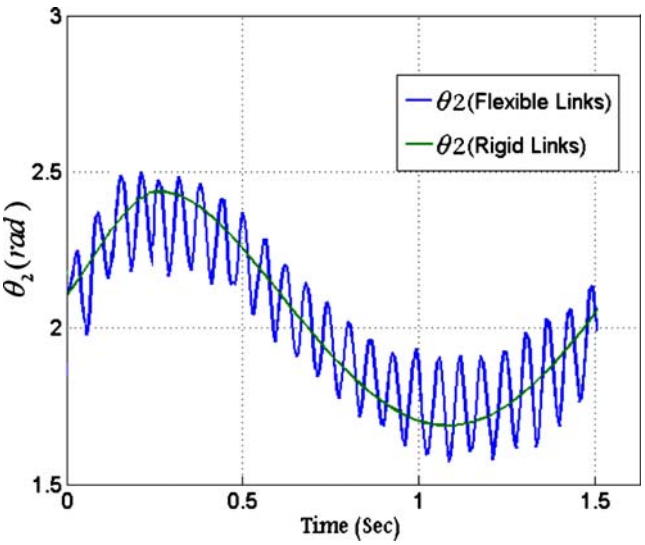

Fig. 14 Joint responses of θ_2 for rigid and flexible links

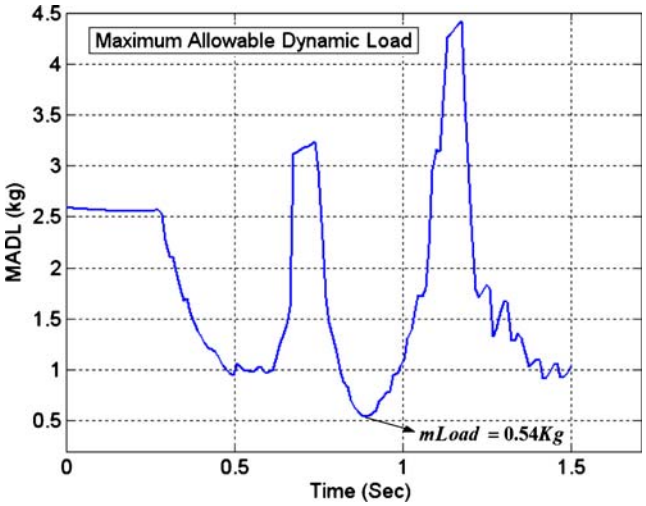

Fig. 15 Maximum allowable dynamic load

Appendix A

A.1 Model development for a two-link manipulator

Consider a two-link flexible manipulator as depicted in Fig. A.1. The mobile base can move in the XY plane, but for the sake of simplicity and avoiding massive computational procedure, only motion in the x-direction is considered as the only degree of freedom of the base in the following computations.

Consider link 1 to be divided into elements '11','12',..., '1j',...'1n_1' of equal length l_1, and link 2 to be divided into elements '21','22',...,'2j',...'2n_2' of equal length l_2. Let us define the following notation where subscript i refers to link i, and subscript ij refer to the *j*th element of link i:

OXY is inertia system of coordinates, $O_iX_iY_i$ is body-fixed system of coordinates attached to link i. u_{2j-1} flexural displacement at the common junction of elements 1(j−1) and 1j of link 1. u_{2j} flexural slope at the tip of common junction of elements '1(j−1)' and '1j' of link 1. This slope is measured with respect to axis O_1X_1. w_{2j-1}, w_{2j} flexural displacement and slope at the common junction of elements '2(j−1)' and '2j' of link 2. This slope is measured with respect to axis O_2X_2 and n_1, n_2 are number of elements of links 1 and 2, respectively.

A.2 Kinetic energy computation

A.2.1 Kinetic energy for an element '1j' of link 1

The kinetic energy T_{1j} for the *j*th element of link 1 may be computed as:

$$T_{1j} = \frac{1}{2}\int_0^{l_1} m_1 \left[\frac{\partial r^T}{\partial t}\cdot\frac{\partial r}{\partial t}\right] dx_{1j} \qquad (A-1)$$

It is convenient to express the vector $\vec{r}$, in terms of a vector $\vec{r}_1$ in the body-fixed system of coordinates $O_1X_1Y_1$ and $\vec{r}_0$ in inertia reference frame.

$$\vec{r} = \vec{r}_0 + T_0^1 \vec{r}_1, \qquad (A-2)$$

where $\vec{r}_0 = \begin{Bmatrix} x_0 \\ 0 \end{Bmatrix}$, $\vec{r}_1 = \begin{bmatrix} (j-1)l_1 + x_{1j} \\ Y_{1j} \end{bmatrix}$, $T_0^1 = \begin{bmatrix} \cos\theta_1 & -\sin\theta_1 \\ \sin\theta_1 & \cos\theta_1 \end{bmatrix}$ and θ_1 is the joint angle between O_1X_1 and OX. The displacement y_{1j} can be described in terms of shape functions of a beam element $\phi_k(x_{1j})$ as:

$$y_{1j}(x_{1j}, t) = \sum_{k=1}^{4} \phi_k(x_{1j}) u_{2j-2+k}(t). \qquad (A-3)$$

$\phi_k(x_{1j})$ can be found in FEM context. From Eqs. (A-2) and (A-3), we have:

$$\frac{\partial r^T}{\partial t}\cdot\frac{\partial r}{\partial t} = \dot{z}_j^T \begin{bmatrix} \left[\frac{\partial r}{\partial x_0}\right]^T \\ \left[\frac{\partial r}{\partial \theta_1}\right]^T \\ \left[\frac{\partial r}{\partial u_{2j-1}}\right]^T \\ \vdots \\ \left[\frac{\partial r}{\partial u_{2j+2}}\right]^T \end{bmatrix} \begin{bmatrix} \frac{\partial r}{\partial x_0} & \frac{\partial r}{\partial \theta_1} & \frac{\partial r}{\partial u_{2j-1}} & \cdots & \frac{\partial r}{\partial u_{2j+2}} \end{bmatrix} \dot{z}_j \qquad (A-4)$$

where $z_j = \begin{bmatrix} x_0 & \theta_1 & u_{2j-1} & u_{2j} & u_{2j+1} & u_{2j+2} \end{bmatrix}^T$. Thus, from Eqs. (A-1) to (A-4), the kinetic energy T_{1j} of element '1j' may be expressed as:

$$T_{1j} = \frac{1}{2}\dot{z}_j^T M_{1j} \dot{z}_j \qquad (A-5)$$

where

$$M_{1j}(i,k) = \int_0^{l_1} m_1 \left(\frac{\partial \vec{r}}{\partial z_{ji}}\right)^T \frac{\partial \vec{r}}{\partial z_{jk}} dx_{1j}, \quad i,\ k = 1,2,...,6 \qquad (A-6)$$

and z_{ji} is the *i*th element of z_j. It can be shown that M_{1j} is:

$$M_{1j} = \begin{bmatrix} M_{1j}(1,1) & M_{1j}(1,2) & \cdots & M_{1j}(1,6) \\ M_{1j}(2,1) & M_{1j}(2,2) & \cdots & M_{1j}(2,6) \\ \vdots & \vdots & & \\ M_{1j}(6,1) & M_{1j}(6,2) & & P_{ij} \end{bmatrix} \qquad (A-7)$$

where P_{ij} is the general mass matrix of beam element which can be found in FEM contexts. Other elements of M_{1j} can be calculated using Eq. (A-6) as follow:

$$M_{1j}(1,1) = m_1 L_1$$
$$M_{1j}(1,2) = m_1 \left(-\frac{l_1^2}{2} - (j-1)l_1^2 \sin\theta_1 - m_1 \cos\theta_1 \vec{\psi}_{1j} \left[\frac{l_1}{2} \quad \frac{l_1^2}{12} \quad \frac{l_1}{2} \quad -\frac{l_1^2}{12}\right]^T \qquad (A-8)$$

with $\psi_{1j} = \begin{bmatrix} u_{2j-1} & u_{2j} & u_{2j+1} & u_{2j+2} \end{bmatrix}$. Other elements of M_{1j} can be found completely in [13].

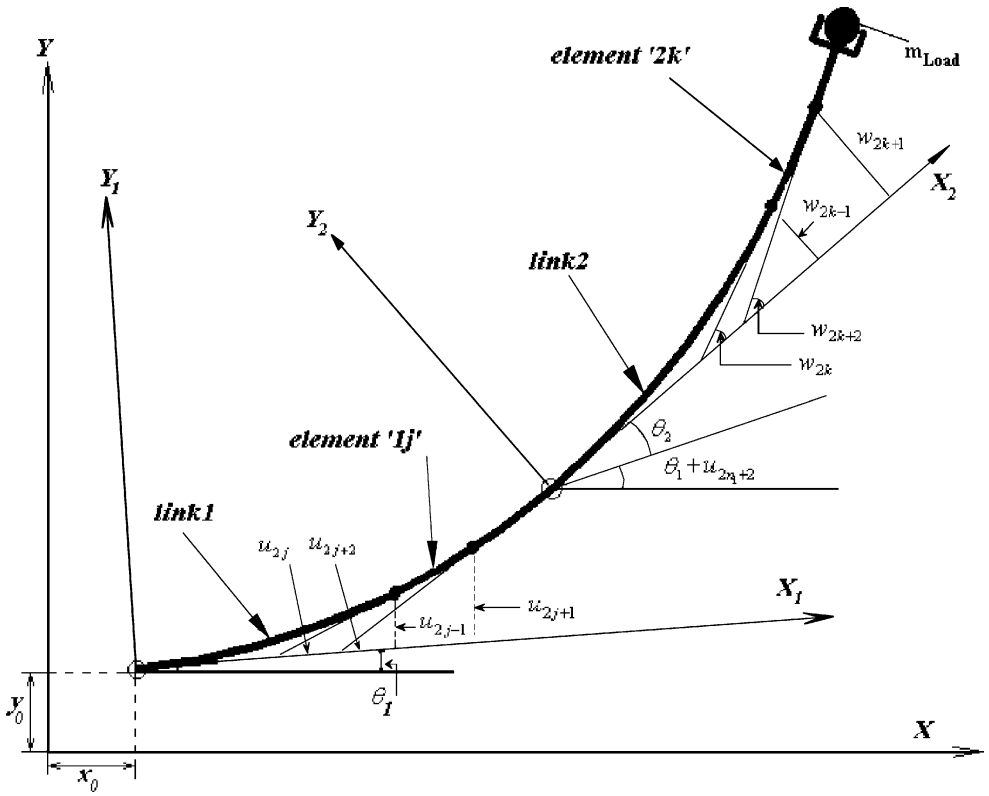

Fig. A.1 Schematic of a two-link flexible mobile manipulator

A.2.2 Total kinetic energy of link 1

As link 1 divided into n_1 elements, the total kinetic energy of link 1 is computed by adding over all elements '1j' of link 1,

$$T_1 = \sum_{j=1}^{n_1} T_{1j} = \sum_{j=1}^{n_1} \frac{1}{2} \dot{z}_j^T M_{1j} \dot{z}_j = \frac{1}{2} \dot{\widetilde{q}}_1^T \widetilde{M}_1 \dot{\widetilde{q}}_1 \qquad (A-9)$$

where

$$\widetilde{q}_1 = \left[x_0, \theta_1, \widetilde{\psi}_1^T\right]^T,$$
$$\widetilde{\psi}_1 = \left[u_1 \;\; u_2 \;\; u_3 \;\; u_4 \;\; \cdots u_{2n_1-1} \;\; u_{2n_1} \;\; u_{2n_1+1} \;\; u_{2n_1+2}\right]^T \qquad (A-10)$$

$\widetilde{M}_1$ is a generalized inertia matrix that is assembled from n mass matrices of n elements for link 1.

A.2.3 Kinetic energy for an element '2j' of link 2

The kinetic energy T_{2j} for *j*th element of link 2 may be computed using Eqs. (A-5) and (A-6) by considering an appropriate $\overrightarrow{r}$ vector as below:

$$\overrightarrow{r} = \begin{Bmatrix} x_0 \\ 0 \end{Bmatrix} + T_0^1 \left[\begin{bmatrix} L_1 \\ u_{2n_1+1} \end{bmatrix} + T_1^2 \begin{bmatrix} (j-1)l_2 \\ y_{2j} \end{bmatrix} \right] \qquad (A-11)$$

where T_0^1 was described in Eq. (A-2). T_1^2 is the transformation matrix between body-fixed system of coordinates, $O_1X_1Y_1$ and $O_2X_2Y_2$ which are attached to the first and second link, respectively, with angle of $\theta_2 + u_{2nl+2}$ (Fig. A.1). y_{2j} may be computed as:

$$y_{2j}(x\ ,t) = \sum_{i=4}^{4} \phi_i(x) W_{2j-2+i}(t), \qquad (A-12)$$

From Eqs. (A-11) to (A-12), it can be concluded that $\overrightarrow{r}$ is independent of u_i for i=1,2,...2n_1.

After some mathematical simplifications and assuming that $q = \theta_2 + u_{2n_1+2}$ and using of extended transformation matrix, we can write the position of each point on *j*th element in the second link as:

$$\overrightarrow{r} = \begin{bmatrix} \cos(\theta_1+q) & -\sin(q+\theta_1) & x_0 \\ \sin(q+\theta_1) & \cos(q+\theta_1) & 0 \\ 0 & 0 & 1 \end{bmatrix} \begin{bmatrix} (j-1)l_2 + x_{2j} \\ y_{2j} \\ 1 \end{bmatrix}$$
$$+ \begin{bmatrix} L_1 \cos\theta_1 - u_{2n_1+1} \sin\theta_1 \\ L_1 \sin\theta_1 + u_{2n_1+1} \cos\theta_1 \\ 0 \end{bmatrix} \qquad (A-13)$$

Then, T_{2j} in Eq. (A-5) may be expressed as:

$$T_{2j} = \frac{1}{2}\dot{z}_j^T M_{2j}\dot{z}_j, \qquad (A-14)$$

where

$$z_j^T = \left[x_0\ \theta_1\ u_{2n_1+1}\ u_{2n_1+2}\ \theta_2\ \psi_{2j}^T\right],\ \textit{and}$$
$$\psi_{2j}^T = \left[w_{2j-1}\ \ w_{2j}\ \ w_{2j+1}\ \ w_{2j+2}\right]. \qquad (A-15)$$

Hence, the mass matrix M_{2j} is a (9×9) matrix which its elements can be computed by the following equation routinely:

$$M_{2j}(i,k) = m_2\int_0^{l_2}\left[\frac{\partial\overrightarrow{r}}{\partial z_{ji}}\right]^T\frac{\partial\overrightarrow{r}}{\partial z_{jk}}dx_{2j} \quad i,\ k = 1,2...9 \qquad (A-16)$$

where z_{ji} is the ith element of z_j.

A.2.4 Total kinetic energy for link 2

The kinetic energy T_2 for link 2 is computed by summing over all elements '2j' of link 2, i.e.,

$$T_2 = \sum_{j=1}^{n_2} T_{2j} = \sum_{j=1}^{n_2}\frac{1}{2}\dot{z}_j M_{2j}\dot{z}_j = \frac{1}{2}\dot{\widetilde{q}}_2^T\widetilde{M}_2\dot{\widetilde{q}}_2 \qquad (A-17)$$

where

$$\widetilde{q}_2 = \left[x_0\ \theta_1\ u_{2n_1+1}\ u_{2n_1+1}\ \theta_2\ \widetilde{\psi}_2^T\right]^T,\ \textit{and}$$
$$\widetilde{\psi}_2 = \left[w_1\ w_2\ \ldots\ w_{2n_2+1}\ w_{2n_2+2}\right]^T.$$

A.3 Potential energy computation

The potential energy for the overall system is obtained by computing the potential energy for each element of the assemblage and adding over all the elements.

A.3.1 Potential energy for a single element '1j' of link 1

Considering OX as the reference, the potential energy V_{1j} of element '1j' of link 1 comprises two components, V_{g1j} due to gravity and V_{e1j} due to elasticity. Considering that the mobility in x_0 direction does not have any effects on V_{1j}, the potential energy of element '1j' of link 1 becomes:

$$V_{1j} = V_{g1j} + V_{e1j} = \int_0^{l_1} m_1 g[0\quad 1]\ T_0^1\begin{bmatrix}(j-1)l_1 + x_{1j}\\ y_{1j}\end{bmatrix}dx_{1j} + \frac{1}{2}\int_0^{l_1} E I_1\left[\frac{\partial^2 y_{1j}}{\partial x_{1j}^2}\right]^2 dx_{1j}. \qquad (A-18)$$

By substituting for y_{1j} from Eq. (A-3) and taking integrative with respect to time, the elemental potential energy becomes:

$$V_{1j} = \frac{1}{2}\psi_{1j}^T k_{1j}\psi_{1j} + m_1 g[0\quad 1]T_0^1\begin{bmatrix}\left(j-\frac{1}{2}\right)l_1^2\\ \frac{l_1}{2}u_{2j-1} + \frac{l_1^2}{12}u_{2j} + \frac{l_1}{2}u_{2j+1} - \frac{l_1^2}{12}u_{2j+2}\end{bmatrix} \qquad (A-19)$$

where ψ_{1j} is defined in Eq. (A-8), and K_{1j} is stiffness matrix of beam element.

A.3.2 Total potential energy for link 1

Since link 1 comprises n_1 elements, its total potential energy is:

$$V_1 = \sum_{j=1}^{n_1} V_{1j} = m_1 g[0\quad 1]T_0^1\begin{bmatrix}\frac{1}{2}n_1^2 l_1^2\\ R_0\widetilde{\psi}_1\end{bmatrix} + \frac{1}{2}\widetilde{\psi}_1^T\widetilde{K}_1\widetilde{\psi}_1 \qquad (A-20)$$

where $\widetilde{\psi}_1$ is defined in Eq. (A-10) and $R_0 = \left[l_1\quad 0|\ |l_1\quad 0|\ \ldots\ |l_1\quad 0|\ \frac{l_1}{2} - \frac{l_1^2}{12}\right]$.

The element of $\widetilde{K}_1$, the general stiffness matrix and can be found in [13].

A.3.3 Potential energy for a single element '2j'

Considering again OX as the reference, the potential energy V_{2j} of the jth element of link 2 is the sum of two

components. One is due to gravity and the other is due to elasticity of system, i.e.,

$$V_{2j} = \int_0^{l_2} m_2 g[0\ \ 1]\left[T_0^1\begin{bmatrix} L_1 \\ u_{2n_1+1}\end{bmatrix} + T_0^1 T_1^2\begin{bmatrix}(j-1)l_2 + x_{2j} \\ y_{2j}\end{bmatrix}\right] dx_{2j} + \frac{1}{2}\int_0^{l_2} EI_2\left[\frac{\partial^2 y_{2j}}{\partial x_{2j}^2}\right]^2 dx_{2j}$$
$$= m_2 g[0\ \ 1]\left[T_0^1\begin{bmatrix} L_1 \\ u_{2n_1+1}\end{bmatrix} l_2 + T_0^1 T_1^2\begin{bmatrix}\left(j-\frac{1}{2}\right)l_2^2 \\ \frac{l_2}{2}w_{2j-1} + \frac{l_2^2}{12}w_{2j} + \frac{l_2}{2}w_{2j+1} - \frac{l_2^2}{2}w_{2j+2}\end{bmatrix}\right] + \frac{1}{2}\psi_{2j}^T K_{2j}\psi_{2j} \qquad (A-21)$$

where ψ_{2j} is given in Eq. (A-15).

A.3.4 Total potential energy for link 2

Summing over all elements '2j' of Link 2, the total potential energy of this link becomes:

$$V_2 = \sum_{j=1}^{n_2} V_{2j}$$
$$= m_2 g[0\quad 1]\left[T_0^1\begin{bmatrix} L_1 \\ u_{2n+1}\end{bmatrix} n_2 l_2 + T_0^1 T_1^2\begin{bmatrix}\frac{1}{2}n_2^2 l_2^2 \\ R_1\psi_2\end{bmatrix}\right]$$
$$+\frac{1}{2}\widetilde{\psi}_2^T\ K_2\ \widetilde{\psi}_2 \qquad (A-22)$$

where $\widetilde{\psi}_2 = [w_1\ \ w_2\ \ \ldots\ \ w_{2n_2+2}]$ and $R_1 = [l_2\ \ 0|\ |l_2\ \ 0|\ \ldots\ |l_2\ \ 0|\ \ \frac{l_2}{2}\ \ -\frac{l_2^2}{12}]$.

The elements of $\widetilde{K}_2$ can be found in [13].

A.4 Boundary condition

In this simulation, it is assumed that the link 1 is constrained to have no displacement and angular displacement at the beginning due to body-fixed axis O_1X_1 (Fig. A.1). It other words, the boundary variables u_1 and u_2 must be zero, i.e., $u_1(t)=0$ and $u_2(t)=0$. The second link has similar boundary condition and has no displacement and angular displacement at the beginning due to O_2X_2. Hence, the constraint variables w_1 and w_2 must be equal to zero, i.e., $w_1(t)=0$ and $w_2(t)=0$. It must be considered that both links have angular displacements θ_1 and θ_2 with their body-fixed axis.

References

1. Thomas M, Yuan-Chou HC, Tesar D (1985) Optimal actuator sizing for robotic manipulators based on local dynamic criteria. J Mech Transm Autom Des 107:163–169
2. Wang LT, Ravani B (1988) Dynamic load carrying capacity of mechanical manipulators. Part I, problem formulation. J Dyn Syst Meas Control 110:46–52
3. Wang LT, Ravani B (1988) Dynamic load carrying capacity of mechanical manipulators. Part II, computational procedure and applications. J Dyn Syst Meas Control 110:53–61
4. Korayem MH, Basu A (1994) Formulation and numerical solution of elastic robot dynamic motion with maximum load carrying capacity. Robotica 12:253–261
5. Korayem MH, Basu A (1994) Dynamic load carrying capacity for robotic manipulators with joint elasticity imposing accuracy constraints. J. of Robotic and Autonomous Systems 13:219–229
6. Yue S, Tso SK, Xu WL (2001) Maximum dynamic payload trajectory for flexible robot manipulators with kinematic redundancy. Mech Mach Theory 36:785–800
7. Korayem MH, Ghariblu H (2003) Maximum allowable load on wheeled mobile manipulators imposing redundancy constraints. J. of Robotic and Autonomous Systems 44(2):151–159
8. Rey DA, Papadopoulos EG (1997) Online automatic tip-over presentation for mobile and redundant manipulators. Proc. of the IEEE International Conference on Intelligent Robots and Systems (IROS'97) 1273–1278
9. Papadopoulos E, Gonthier Y (1999) A frame force for large force task planning of mobile and redundant manipulators. J Robot Syst 16(3):151–162
10. Seraji H (1998) A unified approach to motion control of mobile manipulators. J. of Robot Research 17(12):107–118
11. Chung PH et al. An extension to operational space for kinematically redundant manipulators: kinematics and dynamics. IEEE International Conference on Robotics and Automation 16 (5):592–596
12. Usoro PB, Nadira R, Mahil (1986) A finite element-lagrange approach to modeling lightweight flexible manipulators. J Dyn Syst Meas Control 108:198–205
13. Heidari A (2005) Maximum dynamic load carrying capacity for flexible robot manipulators with finite element approach. M.Sc. Thesis, Mechanical Engineering Department, Iran University Science and Technology, October 2005